© 2017. Published by The Company of Biologists Ltd | Development (2017) 144, 3840-3846 doi:10.1242/dev.149807

A fluorescent toolkit for spatiotemporal tracking of apoptotic cells in living *Drosophila* tissues

Sonia Schott, Arnaud Ambrosini*, Audrey Barbaste*, Corinne Benassayag*, Mélanie Gracia*, Amsha Proag*, Mégane Rayer*, Bruno Monier‡ and Magali Suzanne‡

ABSTRACT

Far from being passive, apoptotic cells influence their environment. For example, they promote tissue folding, myoblast fusion and modulate tumor growth. Understanding the role of apoptotic cells necessitates their efficient tracking within living tissues, a task that is currently challenging. In order to easily spot apoptotic cells in developing *Drosophila* tissues, we generated a series of fly lines expressing different fluorescent sensors of caspase activity. We show that three of these reporters (GFP-, Cerulean- and Venus-derived molecules) are detected specifically in apoptotic cells and throughout the whole process of programmed cell death. These reporters allow the specific visualization of apoptotic cells directly within living tissues, without any post-acquisition processing. They overcome the limitations of other apoptosis detection methods developed so far and, notably, they can be combined with any kind of fluorophore.

KEY WORDS: Apoptosis, Caspase-activity sensor, *Drosophila*, Live imaging

INTRODUCTION

The main function of epithelia is to form and maintain a physical barrier between different compartments of the body. Within epithelia, cells are highly polarized and organized in monolayers. They are connected by adhesive complexes such as apical tight junctions and adherens junctions, as well as basal focal adhesions. This organization ensures tissue integrity, a characteristic that needs to be maintained but is constantly challenged by cell division, cell death or cell intercalation. An epithelium has to deal constantly with the plasticity required to allow tissue growth and remodeling on the one hand and the maintenance of tissue cohesiveness on the other. In recent years, live imaging has become a crucial tool with which to identify cellular mechanisms involved in tissue plasticity.

Recent work has revealed that cells dying through programmed cell death (or apoptosis) can influence their environment either through biochemical communication or through the generation of mechanical forces (for reviews see Ambrosini et al., 2016; Pérez-Garijo and Steller, 2015; Suzanne and Steller, 2013). For example, apoptotic cells play an important role in the remodeling of epithelia, such as during *Drosophila* dorsal closure, histoblast expansion or mouse neural closure (Teng et al., 2017; Toyama et al., 2008; Yamaguchi et al., 2011). More recently, we have provided evidence that apoptotic cells of a columnar epithelium produce an apicobasal force that leads to tissue folding in the fly developing leg (Monier et al., 2015). Apoptotic cells also play a key role in vertebrate myoblast fusion and promote the growth of some tumors (Ford et al., 2015; Hochreiter-Hufford et al., 2013; Huang et al., 2011). Altogether, it is becoming clear that apoptotic cells communicate with their surroundings, which highlights the importance of studying apoptosis in an integrated model system. Understanding the role of apoptotic cells during developmental events makes it necessary to identify them easily and unambiguously, as well as to finely characterize their dynamics. Such a task has been particularly challenging so far because epithelial cells within living tissues are tightly packed. Furthermore, cells undergoing apoptosis progressively disappear, which narrows the window of observation.

Apoptosis is orchestrated by the hierarchical activation of cysteine proteases known as caspases that promote the sequential dismantling of doomed cells (Crawford and Wells, 2011). In *Drosophila*, death signals, such as expression of the proapoptotic genes *reaper* (*rpr*), *hid* or *grim*, trigger the degradation of the anti-apoptotic molecule Diap1, therefore promoting activation of upstream caspases (such as Dronc), which in turn activates effector caspases such as Dcp1 or Drice that usually cleave DEVD sequences (Fuchs and Steller, 2015). *Drosophila* is a model of choice for studying both the role and dynamics of apoptotic cells, yet available tools to track apoptosis in living tissues remain scarce. Doomed cells can be spotted using TUNEL staining or antibodies specific to activated caspases or to caspase targets, but this approach restricts the analysis to fixed tissues (Sarkissian et al., 2014; Williams et al., 2006). Additional methods have been developed to follow caspase activation (Arama and Steller, 2006; Bardet et al., 2008; Ding et al., 2016; Koto et al., 2009; Takemoto et al., 2003; Tang et al., 2015; To et al., 2015), yet all of them have limitations. So far, they provide only limited access to apoptotic cell dynamics either because they require post-acquisition image processing, such as FRET analysis, because they only detect late apoptotic cells or because they are activated in all cells that experience caspase activation whether they die or not (see Fig. S1). This prompted us to investigate whether alternative methods of detection of caspase activity could be implemented in *Drosophila* to easily follow the dynamics of dying cells in living tissues.

Interestingly, Li and co-workers (Zhang et al., 2013) recently generated four cyclized chimera proteins containing a caspase 3 cleavage site that behave as switch-on fluorescent-based indicators of apoptosis in cultured mammalian cells. When cleaved by a caspase3-like protease, the non-fluorescent indicator becomes rapidly fluorescent and thus detects the activation of such caspases (DEVDases) in real-time (Fig. 1A; Fig. S2). We have adapted these constructs to the *Drosophila* model. Here, we show that three of these fluorescent-based constructs allow efficient

LBCMCP, Centre de Biologie Intégrative (CBI), Université de Toulouse, CNRS/UPS, 118 route de Narbonne, 31062 Toulouse, France.
*These authors contributed equally to this work

‡Authors for correspondence (magali.suzanne@univ-tlse3.fr; bruno.monier@univ-tlse3.fr)

B.M., 0000-0002-3553-6396; M.S., 0000-0003-0801-3706

Received 31 January 2017; Accepted 29 August 2017

Development (2017) 144, 3840-3846 doi:10.1242/dev.149807

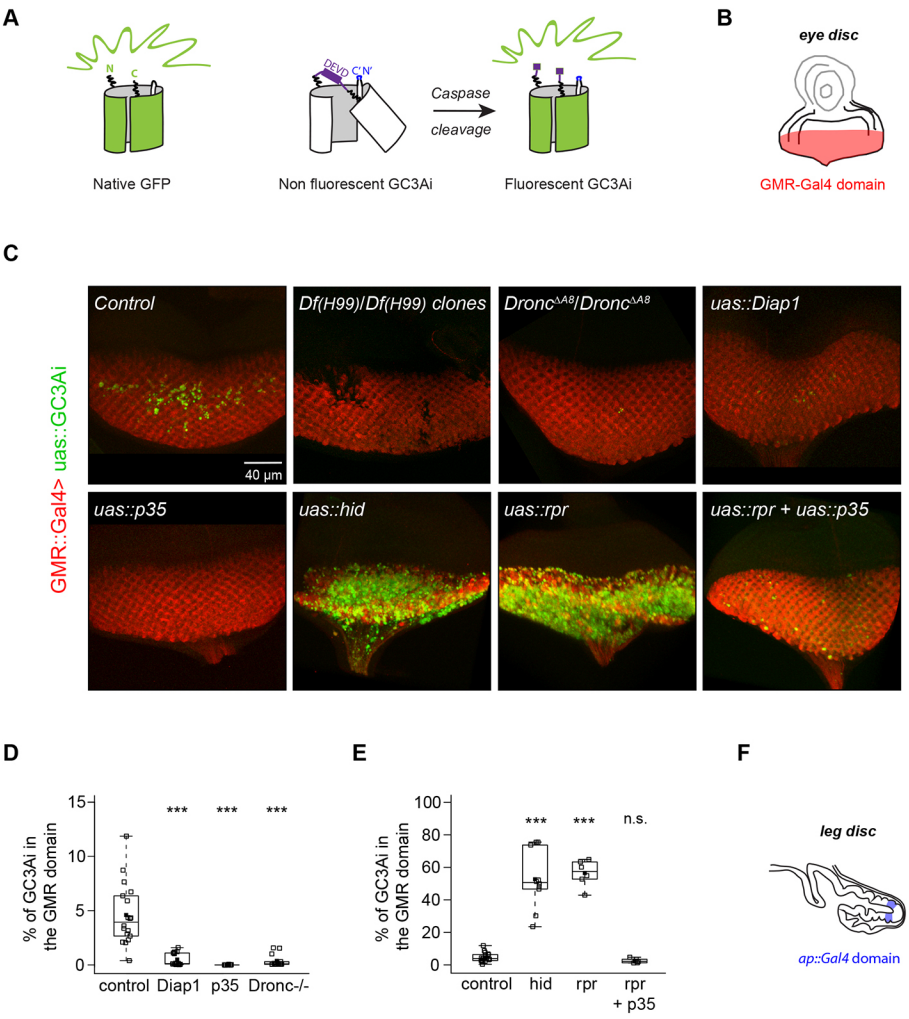

Fig. 1. GC3Ai, a GFP sensor responding to the apoptotic pathway in *Drosophila*. (A) Scheme of the GFP sensor caspase-3-like protease activity indicator (GC3Ai): the C and N termini of the GFP have been linked by a fragment containing a DEVD caspase cleavage site in such a way that DEVD needs to be cleaved in order for the GFP to fluoresce (see Fig. S2 or Zhang et al., 2013 for a more detailed description). (B) Scheme of the L3 eye-antennal disc showing the GMR-Gal4 expression domain. (C) Fixed eye discs from L3 larvae showing the pattern of GC3Ai fluorescence (green) in the *GMR::Gal4* expression domain. In all the indicated genetic contexts, the whole GMR domain is labeled in red by the detection of GC3Ai expression with an anti-GFP antibody (detecting both the active and inactive conformations of GC3Ai), except in the H99 mutant context, in which GC3Ai is expressed only in the mutant clones. (D,E) Quantification of GC3Ai fluorescence within the GMR expression domain in the different genotypes illustrated in C. Individual eye discs (open squares) as well as the mean (closed square) are shown on the box plots. ***P<0.005; n.s., non-significant. In C, D and E, the number of discs analyzed was: control (18); *uas::Diap1* (14); *uas::p35* (16); *uas::hid* (10); *uas::rpr* (6); *uas::rpr+ uas::p35* (6); *DroncΔA8/DroncΔA8* (14); and *Df (H99) /Df(H99)* (8). (F) Scheme of a pupal leg disc showing the *ap::Gal4* expression pattern in blue. (G) A fixed pupal leg disc (n=10 legs) showing the pattern of GC3Ai fluorescence (green and white) in the *ap* domain and Dcp1 activity in the whole leg (red and white). Anti-GFP antibody is in blue. Apoptotic cells located in the *ap* domain show both GC3Ai and Dcp1 activity (arrows), whereas only Dcp1 is detected in those located outside the *ap* domain (arrowheads).

detection of apoptotic cells within a whole tissue (fixed or live), both in normal developmental conditions or after apoptosis induction. We therefore introduce new tools that allow easy visualization of the whole apoptotic process within living *Drosophila* tissues, from the very beginning of the apoptotic process to cell fragmentation and formation of apoptotic bodies. Moreover, the possibility to combine apoptosis detection with any other fluorescent fusion protein makes these sensors particularly useful.

RESULTS AND DISCUSSION

A new tool to detect the activity of caspases in *Drosophila*: the GFP sensor GC3Ai

In order to determine whether the GFP-based variant of caspase 3-like proteases activity indicator (GC3Ai, Fig. 1A) is an efficient reporter of the activation of the apoptotic pathway in *Drosophila*, as it is in mammalian cells in culture, we generated stable transgenic *UAS::GC3Ai* fly lines. First, we asked whether the expression of this construct per se leads to potential side effects. We could show that its ubiquitous expression has little impact on viability (see Fig. S3A). Furthermore, comparison of the level of apoptosis in presence or in absence of *UAS::GC3Ai* demonstrates that this molecule has little effect, if any, on the rate of apoptosis (see Fig. S3B,C). We next characterized the pattern of GC3Ai fluorescence (hereafter called the activation pattern) by expressing GC3Ai in the eye using the *GMR::Gal4* driver (Fig. 1B). GC3Ai is detected in a small number of cells within the eye disc (Fig. 1C, control), a pattern reminiscent of the apoptotic pattern in this tissue (White et al., 1996). As expected, GC3Ai activation is abolished in cells that are homozygous mutant for the H99 deficiency (which removes the three pro-apoptotic genes *hid*, *rpr* and *grim*) or for the activator caspase *Dronc* (Fig. 1C,D). GC3Ai activation also disappears if apoptosis is blocked either by the expression of the anti-apoptotic factor Diap1 [which suppresses apoptosis by blocking both activator and effector caspases (Hay et al., 1994)] or p35 [which

Development (2017) 144, 3840-3846 doi:10.1242/dev.149807

blocks only effector caspases (Hay et al., 1995)] (Fig. 1C,D). Conversely, expression of the pro-apoptotic genes *rpr* or *hid* greatly increases the activation domain of GC3Ai, reaching around 50 to 60% of the whole GMR domain (Fig. 1C,E). Finally, if p35 is co-expressed with Rpr, the activation of GCA3i diminishes drastically (Fig. 1C,E). Altogether, these results indicate that GC3Ai activity responds to the apoptotic machinery in the fly, as it does in mammalian cells (Zhang et al., 2013). Furthermore, the fact that GC3Ai activity is fully suppressed by p35 (Fig. 1C,D,E), which does not inhibit activator caspases (Hay et al., 1995), suggests that the GC3Ai biosensor reports essentially, if not only, the activity of effector caspases.

As the experiments presented above suggest that the GC3Ai apoptosensor is activated by effector caspases, we hypothesized that GC3Ai staining should colocalize with staining of activated effector caspases in fixed tissues. We therefore expressed GC3Ai in the leg disc at the onset of metamorphosis using the *ap::Gal4* driver (Fig. 1F), a tissue in which the pattern and morphology of dying cells have previously been described (Monier et al., 2015). We counterstained with an antibody against the active form of the effector caspase Dcp1 (Sarkissian et al., 2014) and found that 99% (±1%) of Dcp1-positive cells are also GC3Ai positive (Fig. 1G, quantifications detailed in the Materials and Methods). Furthermore, we show that GC3Ai and the active form of Dcp1 are both detected in the same population of cells in a variety of tissues at distinct developmental stages, ranging from the embryonic ectoderm to larval tissues (imaginal discs and brain) and the pupal notum (Fig. S4). Altogether, our results indicate that GC3Ai efficiently detects apoptotic cells, thus validating the construct as a GFP apoptosensor in *Drosophila*.

GC3Ai is an efficient tool with which to follow apoptotic cell dynamics

In order to assess the suitability of GC3Ai for live imaging, we expressed and imaged it in the developing leg, a tissue in which apoptotic dynamics has been previously characterized using a FRET probe (Monier et al., 2015). Importantly, we found that the signal-to-noise ratio was high, even at low laser power, indicating that GC3Ai is adequate for good quality detection of apoptotic cells *in vivo* in optimal conditions for tissue culture. We therefore followed apoptotic cell dynamics *in vivo* and found that fluorescent GC3Ai is strongly and specifically detected in apoptotic cells, from a very early stage until cell fragmentation (Fig. 2A,B, Movie 1). Interestingly, the strong cytoplasmic signal obtained with GC3Ai makes it possible to follow the whole process of apoptotic cell

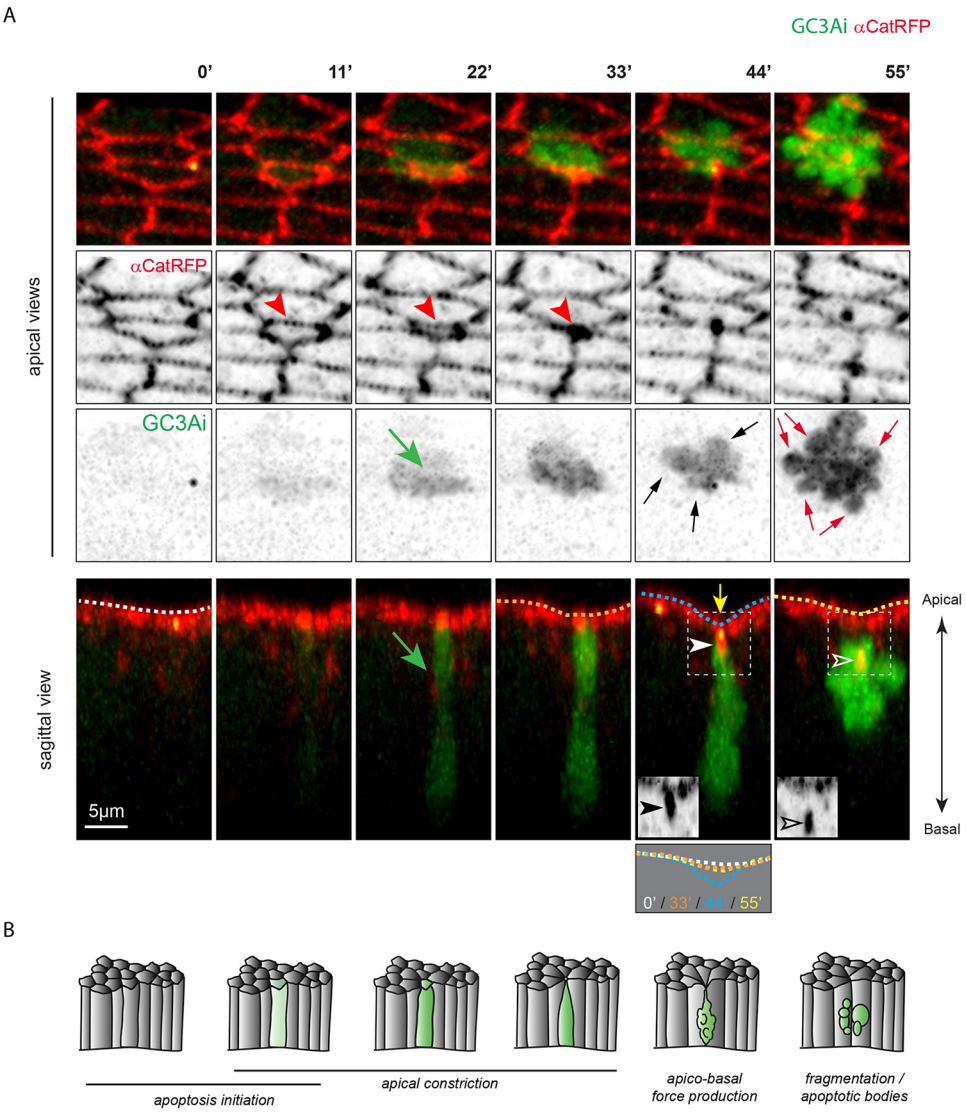

Fig. 2. Dynamics of GC3Ai pattern of fluorescence in a living tissue.
(A) Confocal images extracted from Movie 1 showing the dynamics of GC3Ai fluorescence (green or black) and alpha-catenin-TagRFP (red or black) in one apoptotic cell of a pupal leg disc (*n*=11). Apical views are presented in the upper panels and the corresponding sagittal sections below. GC3Ai activation (green arrows) is detected before the completion of apical constriction (red arrowheads). Black and red arrows indicate, respectively, blebs and apoptotic bodies. In sagittal sections, arrowheads indicate apoptotic adherens junction accumulation, before (closed) and after (open) detachment. Apical deformation is highlighted with a yellow arrow and apical surface drawings (dashed lines).
(B) Schemes of the apoptotic stages visualized in A, summarizing the dynamics of the GC3Ai activation pattern *in vivo*.

Development (2017) 144, 3840-3846 doi:10.1242/dev.149807

morphological changes in detail. This includes a first step of apical constriction of the apoptotic cell (Fig. 2A, red arrowheads, 11′ to 33′), which culminates with adherens junction accumulation in the dying cell underneath yet in continuity with the adherens junctions of neighboring living cells (Fig. 2A, black and white arrowheads, 44′). At the same timepoint, apoptotic cell blebbing (Coleman et al., 2001) is visualized as round unfragmented protrusions (Fig. 2A, black arrows, 44′) while apical surface deformation of living neighboring cells (Fig. 2A, yellow arrow, superposition of dashed lines) reveals the generation of a transient apico-basal apoptotic force (Monier et al., 2015). The GC3Ai signal perdures right up to cell fragmentation (red arrows) which occurs concomitantly with detachment of the apoptotic adherens junctions (Fig. 2A, open arrowheads, 55′). Hence, apoptotic cell tracking through GC3Ai recapitulates the known morphological behavior of apoptotic cells in the leg disc, which has been initially visualized using the FRET sensor of caspase activity (Monier et al., 2015; Takemoto et al., 2003). Interestingly, both GC3Ai and the FRET sensor detect early events of the apoptotic process (detection of the apoptotic cells during apical constriction); however, GC3Ai surpasses the FRET probe in several aspects. First, it provides the ability to directly visualize an apoptotic cell under the microscope, whereas the FRET probe requires post-acquisition treatment to spot a dying cell. GC3Ai also allows 3D rendering of the cellular morphology of dying cells. Supporting this, individual apoptotic fragments can be counted and quantified using GC3Ai, which is extremely difficult or even impossible solely on the basis of the FRET probe (Fig. S5).

We next characterized the pattern of GC3Ai in fixed tissues. Interestingly, GC3Ai can be detected early during the apoptotic process, as shown by its detection in columnar cells, before the completion of apical constriction, a stage at which it is not possible to detect apoptotic cells using conventional tools such as anti-activated Dcp1 staining (Fig. 3, 'apoptosis initiation'). We further demonstrated that more apoptotic fragments can be detected with GC3Ai than with Dcp1 staining, showing that GC3Ai allows detection of late apoptotic stages that cannot be analyzed using conventional strategies (Fig. 3, 'apoptotic bodies'). Altogether, these results reveal that the GC3Ai pattern of activation is similar in both fixed and living tissues. GC3Ai is an efficient sensor of apoptosis that possesses an even higher sensitivity than Dcp1 in fixed tissues and allows real-time *in vivo* analysis, making GC3Ai a versatile tool with which to study apoptotic cell dynamics in the fly.

Additional fluorophores implement the apoptosensor toolkit

To further implement the apoptosensor toolkit, we generated UAS lines with three other fluorescent versions of the apoptosensor initially developed by Li and colleagues (mCherry-, Cerulean- and Venus-derived constructs, respectively RC3Ai, CC3Ai and VC3Ai) (Zhang et al., 2013). We tested these different lines by expressing them in the developing leg. Expression of the *UAS-RC3Ai* transgene leads to the formation of aggregates in all cell types (apoptotic or not), indicating that this C3Ai variant is inadequate to report apoptosis in the fly (data not shown). Alternative strategies, such as the one recently developed by To and colleagues (To et al., 2016) to label apoptotic cells in zebrafish could be considered in the future to engineer a red apoptosensor in *Drosophila*.

To characterize CC3Ai and VC3Ai constructs, we first combined them with GC3Ai and expressed them in the leg disc. Sequential detection of each one of these constructs with specific filters show that they are suitable for live imaging (good quality detection with low laser power). As expected, CC3Ai and VC3Ai are detected in apoptotic cells, as shown by their co-detection with GC3Ai (Fig. 4A,B).

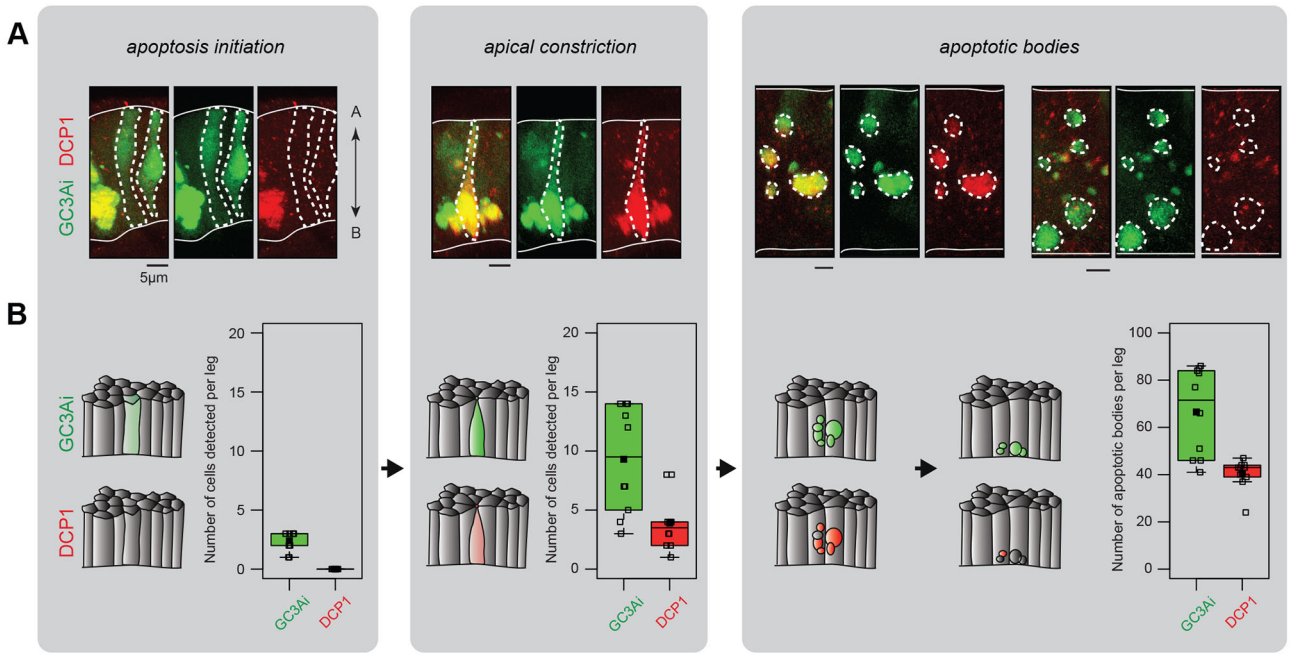

Fig. 3. GC3Ai is specifically detected in apoptotic cells. (A,B) GC3Ai (green) and Dcp1 (red) activation patterns are compared in fixed pupal leg discs at successive stages of the apoptotic process (left to right) using confocal images (A) or quantifications (B). In A, apoptotic cells or fragments are surrounded by white dotted lines, and apical and basal surfaces of the epithelium are represented by a white line. (B) Quantification of the number of GC3Ai- and Dcp1-positive apoptotic cells or apoptotic bodies per leg disc (n=10 legs). Individual leg discs (open squares) as well as the mean (closed square) are shown on the box plots. Schemes of the different apoptotic stages recapitulating the activation pattern of GC3Ai and Dcp1 are presented on the left.

Development (2017) 144, 3840-3846 doi:10.1242/dev.149807

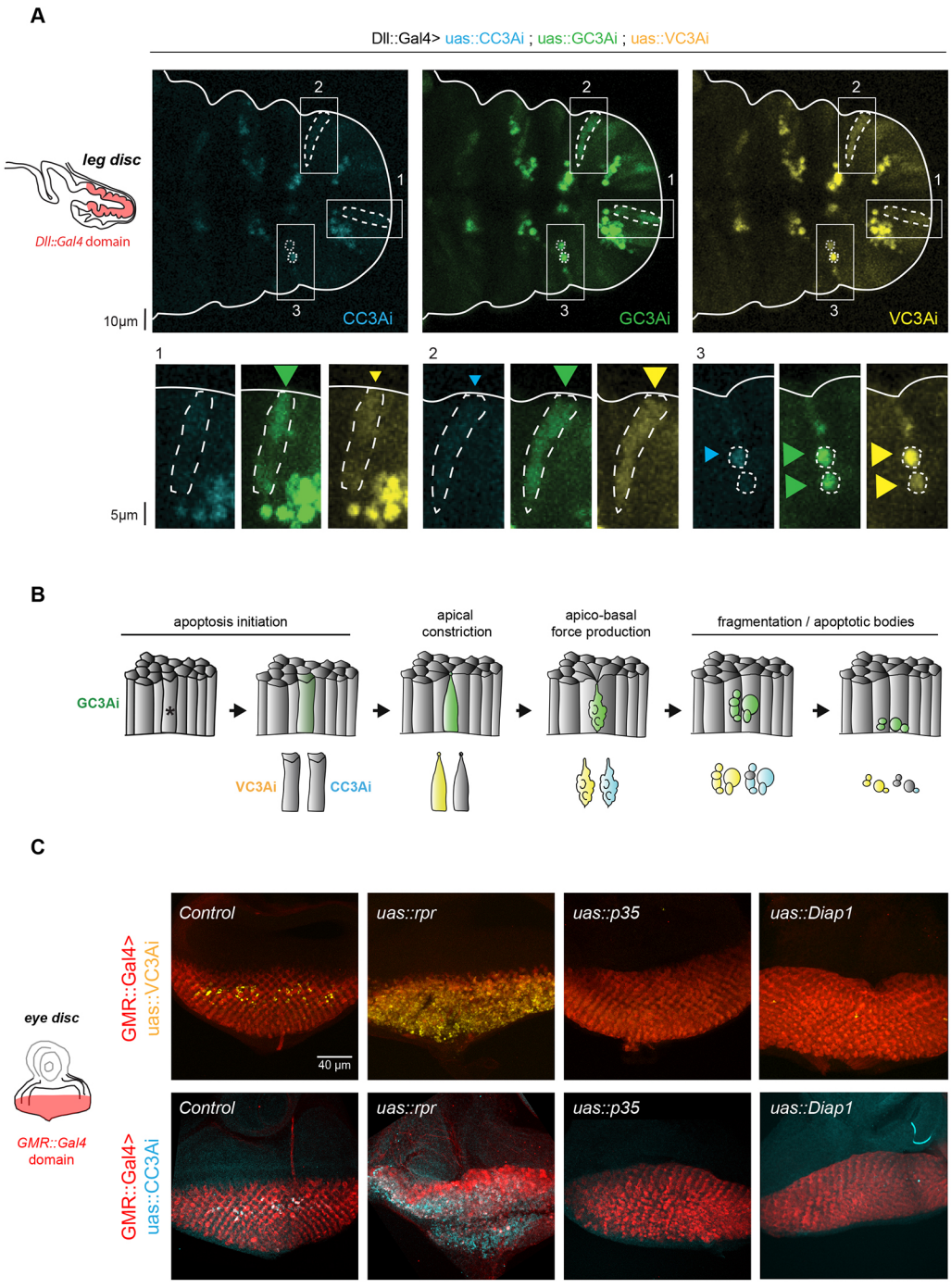

Fig. 4. Characterization of Cerulean and Venus apoptosensors in *Drosophila* tissues. (A) Comparison of GC3Ai, VC3Ai and CC3Ai patterns of fluorescence in the same living leg disc (n=8 legs). Different filters were used to detect the different fluorophores in optimal conditions. Areas 1, 2 and 3 correspond to different apoptotic stages and show the temporal shift in the detection of each sensor, GC3Ai being detected first at an early stage (1, green arrowhead), while VC3Ai is barely detectable (1, yellow arrowhead) and CC3Ai is absent; then VC3Ai is detected (2, yellow arrowhead), while CC3Ai is barely detectable. Finally, GC3Ai and VC3Ai are strongly detected in apoptotic bodies, while CC3Ai is only visible in some fragments (3). (B) The dynamics of GC3Ai, VC3Ai and CC3Ai patterns of fluorescence in living tissues. (C) Fixed eye discs from L3 larvae showing the pattern of CC3Ai and VC3Ai fluorescence (cyan and yellow, respectively) in the *GMR::Gal4* expression domain in the indicated genetic contexts. The number of discs analyzed was: control (10 and 8); uas::Diap1 (8 and 11); uas::p35 (9 and 10); uas::rpr (7 and 7), respectively, for VC3Ai and CC3Ai.

We noted, however, that VC3Ai appears to be detected earlier (during the completion of apical constriction) than CC3Ai, which is weakly or not detected in early apoptotic cells (Fig. 4A,B). We further checked that CC3Ai and VC3Ai are co-detected in Dcp1-positive cells in fixed tissues and quantified the proportion of VC3Ai- and CC3Ai-positive cells at different apoptotic stages (Fig. S6). In summary, the three constructs differ slightly in their temporal detection, appearing successively during the apoptotic process: first GC3Ai, then VC3Ai followed by CC3Ai. Finally, we tested their sensitivity to the apoptotic pathway by analyzing their activation pattern in the imaginal eye disc in different genetic contexts. Similarly to GC3Ai, ectopic expression of *rpr* leads to strong activation of CC3Ai and VC3Ai, while blocking apoptosis using *Diap1* or *p35* expression abolishes their activation (Fig. 4C). These results validate the use of CC3Ai or VC3Ai as alternative apoptosis reporters to GC3Ai.

To conclude, the apoptosensors described here offer the opportunity to recognize caspase activity and apoptotic cells directly within *Drosophila* tissues. These tools do not require post-acquisition processing and can be used either in fixed or living samples, bypassing the potential limitation of antibodies. These constructs detect a wide range of apoptotic stages and constitute excellent tools for following apoptotic cell dynamics within living tissues, particularly GC3Ai, which surpasses the detection range of Dcp1. Finally, the possibility of combining these apoptosensors with any other fluorescent marker provides a considerable stepping stone for analyzing the dynamics of tagged cellular components in apoptotic cells.

Development (2017) 144, 3840-3846 doi:10.1242/dev.149807

MATERIALS AND METHODS

Cloning

CC3Ai, GC3Ai, VC3Ai and RC3Ai cDNAs (a gift from Binghui Li's Lab, Tianjin Medical University Cancer Institute and Hospital, China) were individually cloned into the *Eco*RI site of pUAST *Drosophila* expression vector (a gift from C. Iampietro, LBCMCP, CBI, France) using the In-Fusion HD Cloning System (Clontech). The forward primer used to amplify the CC3Ai, GC3Ai, VC3Ai and RC3Ai cDNAs (including HA tag) was AG-GGAATTGGGAATTCGCCACCATGTACCCCTACGACGTG. The reverse primer used to amplify CC3Ai, GC3Ai and VC3Ai (including Myc tag) was ATCTGTTAACGAATTCCGCTTACAGGTCCTCCTCGCTGATC. The reverse primer used to amplify RC3Ai was ATCTGTTAACGAATTC-GCGGCCGCTTACACATTAATACTA.

Genetics

pUAST-CC3Ai, pUAST-GC3Ai, pUAST-VC3Ai and pUAST-RC3Ai were generated in this study. P-element transformations were performed by the CBMSO *Drosophila* Transgenesis Service (Madrid, Spain) using random insertion in a *white* background. Insertions were recovered on each chromosome.

Apoptosensor expression was achieved using the following Gal4 lines from Bloomington: *ap::Gal4[md544]*, *Dll::Gal4[EM212]*, *act5c::Gal4*, *hh::Gal4, en::Gal4, Tub::Gal4* and *GMR::Gal4*. Manipulation of apoptosis was performed using *uas::rpr*, *uas::p35*, *uas::Diap1-H*, *uas::Diap1-P*, *uas::hid[4]* and *uas::rpr; uas::p35* (a gift from H. Steller, Rockefeller University, USA). *UAS::Histone2Av-mKO* was crossed to *GMR::Gal4* and used as a control in the experiments reported in Fig. 1. *UAS::alphaCatenin-TagRFP* was a gift from K. Sugimura (iCeMS, Japan). Unless noted, stocks were obtained from Bloomington Drosophila Stock Center (BDSC). ubi::mCD8-DQVD-Gal4 and G-TRACE flies were obtained from M. Hardwick and D. Montell (Johns Hopkins Medicine, USA; UC Santa Barbara, USA) (Ding et al., 2016; Tang et al., 2015). $Dronc^{\Delta A8}$ and $Drice^{\Delta 2C8}$ mutants (Kondo et al., 2006) were gifts from M. Miura (University of Tokyo, Japan). Analysis of GC3Ai expression in absence of *hid*, *rpr* and *grim* was achieved by crossing GMR::Gal4, uas::GC3Ai; Df(3L)H99, FRT2A flies with ey::Flp; ; tub::Gal80, FRT2A flies. In this context, GMR::Gal4 is expressed only in $Df(H99)^{-/-}$ clones, which can be labeled positively by anti-GFP staining.

Imaging

Leg discs dissection, immunostaining and *ex vivo* cultures were performed as previously described (Monier et al., 2015). Embryo staining was performed as described previously (Monier et al., 2010). Confocal images were acquired using a Zeiss LSM880 confocal using 25×/0.8 immersion and 40×/1.3 immersion objectives.

Antibodies and probes used were: rabbit anti-cleaved Dcp1 #9578 (1/200, Cell Signaling Technologies); rabbit anti-GFP #ab290 (1/500, Abcam); chicken anti-GFP #1020 (1/1000, Avès lab); phalloidin-rhodamine (1/200, Invitrogen); and phalloidin-Alexa647 (1/100, Interchim). Secondary antibodies coupled to Cy5 were obtained from Jackson Laboratories and diluted 1/50.

Endogenous fluorescence of CC3Ai, GC3Ai and VC3Ai is detected directly following excitation at 405 nm or 458 nm to visualize Cerulean, 488 nm for superfolderGFP or 514 nm for Venus. Non-fluorescent GC3Ai (i.e. GC3Ai in non apoptotic cells) can be detected in fixed tissues using rabbit or chicken polyclonal antibody against GFP. FRET and FM4-64 membrane stainings were performed and analyzed as described previously (Monier et al., 2015).

Quantifications

To quantify the number of apoptotic cells and fragments in pupal leg discs, 3D image stacks were reconstructed using Imaris software (Bitplane) and smoothed using a 3 voxel-large median filter. Fluorescent objects (cells and apoptotic bodies) were segmented on each channel separately (Dcp1, CC3Ai, VC3Ai and GC3Ai, respectively) using the Imaris Surface tool with a manual threshold. Only objects larger than 4 μm^3 were included in the count. To quantify the number of GC3Ai-positive apoptotic cells and fragments within the Dcp1-positive population, we considered objects with at least a 50% overlap over the Dcp1 and GC3Ai channels.

To quantify the response of GC3Ai to the apoptotic machinery in the imaginal eye (Fig. 1), discs were stained with rabbit anti-GFP to reveal the domain of GMR expression. 3D image stacks were reconstructed using Imaris software (Bitplane). Channels corresponding to endogenous GC3Ai fluorescence and the GMR::Gal4 domain were segmented separately, as indicated above. The overall volume of GC3Ai endogenous fluorescence was normalized by the overall volume of the domain for each eye disc.

Statistics

On all graphs, data are presented as box plots with median, lower and upper quartiles, whiskers extending to 1.5 times the interquartile range, mean and individual measurements. Statistical comparison of GC3Ai fluorescence in the *GMR::Gal4* domain across conditions (Fig. 1D,E) or Dcp1 staining in *en::Gal4* domain across conditions (Fig. S3C) were assessed using the Wilcoxon-Mann–Whitney rank-sum test. Asterisks indicate statistical significance: *** $P<0.005$.

Acknowledgements

We thank Binghui Li for sharing the sensor constructs; M. Hardwick, M. Miura, D. Montell and H. Steller for sharing stocks; E. Martin for comments on the manuscript; and the Bloomington Drosophila Stock Center (NIH P40OD018537) for numerous stocks used in this study.

Competing interests

The authors declare no competing or financial interests.

Author contributions

Conceptualization: B.M., M.S.; Methodology: B.M., M.S.; Validation: A.A., A.B., C.B., M.G., A.P., M.R., B.M., M.S.; Formal analysis: A.P.; Investigation: S.S., A.A., A.B., C.B., M.G., A.P., M.R., B.M., M.S.; Writing - original draft: B.M., M.S.; Writing - review & editing: A.P., B.M., M.S.; Supervision: S.S., B.M., M.S.; Funding acquisition: M.S.

Funding

This project has received funding from the European Research Council (ERC) under the European Union Horizon 2020 research and innovation program (grant number EPAF: 648001), from the Fondation ARC pour la Recherche sur le Cancer (CA 09-12-2014) and from Institut National de la Santé et de la Recherche Médicale (Plan Cancer 2014-2019).

Supplementary information

Supplementary information available online at
http://dev.biologists.org/lookup/doi/10.1242/dev.149807.supplemental

References

Ambrosini, A., Gracia, M., Proag, A., Rayer, M., Monier, B. and Suzanne, M. (2016). Apoptotic forces in tissue morphogenesis. *Mech. Dev.* **144**, 33-42.

Arama, E. and Steller, H. (2006). Detection of apoptosis by terminal deoxynucleotidyl transferase-mediated dUTP nick-end labeling and acridine orange in Drosophila embryos and adult male gonads. *Nat. Protoc.* **1**, 1725-1731.

Bardet, P.-L., Kolahgar, G., Mynett, A., Miguel-Aliaga, I., Briscoe, J., Meier, P. and Vincent, J.-P. (2008). A fluorescent reporter of caspase activity for live imaging. *Proc. Natl. Acad. Sci. USA* **105**, 13901-13905.

Coleman, M. L., Sahai, E. A., Yeo, M., Bosch, M., Dewar, A. and Olson, M. F. (2001). Membrane blebbing during apoptosis results from caspase-mediated activation of ROCK I. *Nat. Cell Biol.* **3**, 339-345.

Crawford, E. D. and Wells, J. A. (2011). Caspase substrates and cellular remodeling. *Annu. Rev. Biochem.* **80**, 1055-1087.

Ding, A. X., Sun, G., Argaw, Y. G., Wong, J. O., Easwaran, S. and Montell, D. J. (2016). CasExpress reveals widespread and diverse patterns of cell survival of caspase-3 activation during development in vivo. *Elife* **5**, e10936.

Ford, C. A., Petrova, S., Pound, J. D., Voss, J. J. L. P., Melville, L., Paterson, M., Farnworth, S. L., Gallimore, A. M., Cuff, S., Wheadon, H. et al. (2015). Oncogenic properties of apoptotic tumor cells in aggressive B cell lymphoma. *Curr. Biol.* **25**, 577-588.

Fuchs, Y. and Steller, H. (2015). Live to die another way: modes of programmed cell death and the signals emanating from dying cells. *Nat. Rev. Mol. Cell Biol.* **16**, 329-344.

Hay, B. A., Wolff, T. and Rubin, G. M. (1994). Expression of baculovirus P35 prevents cell death in Drosophila. *Development* **120**, 2121-2129.

Hay, B. A., Wassarman, D. A. and Rubin, G. M. (1995). Drosophila homologs of baculovirus inhibitor of apoptosis proteins function to block cell death. *Cell* **83**, 1253-1262.

Development (2017) 144, 3840-3846 doi:10.1242/dev.149807

Hochreiter-Hufford, A. E., Lee, C. S., Kinchen, J. M., Sokolowski, J. D., Arandjelovic, S., Call, J. A., Klibanov, A. L., Yan, Z., Mandell, J. W. and Ravichandran, K. S. (2013). Phosphatidylserine receptor BAI1 and apoptotic cells as new promoters of myoblast fusion. *Nature* **497**, 263-267.

Huang, Q., Li, F., Liu, X., Li, W., Shi, W., Liu, F.-F., O'Sullivan, B., He, Z., Peng, Y., Tan, A.-C. et al. (2011). Caspase 3-mediated stimulation of tumor cell repopulation during cancer radiotherapy. *Nat. Med.* **17**, 860-866.

Kondo, S., Senoo-Matsuda, N., Hiromi, Y. and Miura, M. (2006). DRONC coordinates cell death and compensatory proliferation. *Mol. Cell. Biol.* **26**, 7258-7268.

Koto, A., Kuranaga, E. and Miura, M. (2009). Temporal regulation of Drosophila IAP1 determines caspase functions in sensory organ development. *J. Cell Biol.* **187**, 219-231.

Monier, B., Pélissier-Monier, A., Brand, A. H. and Sanson, B. (2010). An actomyosin-based barrier inhibits cell mixing at compartmental boundaries in Drosophila embryos. *Nat. Cell Biol.* **12**, 60-65; sup pp 61-69.

Monier, B., Gettings, M., Gay, G., Mangeat, T., Schott, S., Guarner, A. and Suzanne, M. (2015). Apico-basal forces exerted by apoptotic cells drive epithelium folding. *Nature* **518**, 245-248.

Pérez-Garijo, A. and Steller, H. (2015). Spreading the word: non-autonomous effects of apoptosis during development, regeneration and disease. *Development* **142**, 3253-3262.

Sarkissian, T., Timmons, A., Arya, R., Abdelwahid, E. and White, K. (2014). Detecting apoptosis in Drosophila tissues and cells. *Methods* **68**, 89-96.

Suzanne, M. and Steller, H. (2013). Shaping organisms with apoptosis. *Cell Death Differ.* **20**, 669-675.

Takemoto, K., Nagai, T., Miyawaki, A. and Miura, M. (2003). Spatio-temporal activation of caspase revealed by indicator that is insensitive to environmental effects. *J. Cell Biol.* **160**, 235-243.

Tang, H. L., Tang, H. M., Fung, M. C. and Hardwick, J. M. (2015). In vivo CaspaseTracker biosensor system for detecting anastasis and non-apoptotic caspase activity. *Sci. Rep.* **5**, 9015.

Teng, X., Qin, L., Le Borgne, R. and Toyama, Y. (2017). Remodeling of adhesion and modulation of mechanical tensile forces during apoptosis in Drosophila epithelium. *Development* **144**, 95-105.

To, T.-L., Piggott, B. J., Makhijani, K., Yu, D., Jan, Y. N. and Shu, X. (2015). Rationally designed fluorogenic protease reporter visualizes spatiotemporal dynamics of apoptosis in vivo. *Proc. Natl. Acad. Sci. USA* **112**, 3338-3343.

To, T.-L., Schepis, A., Ruiz-González, R., Zhang, Q., Yu, D., Dong, Z., Coughlin, S. R. and Shu, X. (2016). Rational design of a GFP-based fluorogenic caspase reporter for imaging apoptosis in vivo. *Cell Chem. Biol.* **23**, 875-882.

Toyama, Y., Peralta, X. G., Wells, A. R., Kiehart, D. P. and Edwards, G. S. (2008). Apoptotic force and tissue dynamics during Drosophila embryogenesis. *Science* **321**, 1683-1686.

White, K., Tahaoglu, E. and Steller, H. (1996). Cell killing by the Drosophila gene reaper. *Science* **271**, 805-807.

Williams, D. W., Kondo, S., Krzyzanowska, A., Hiromi, Y. and Truman, J. W. (2006). Local caspase activity directs engulfment of dendrites during pruning. *Nat. Neurosci.* **9**, 1234-1236.

Yamaguchi, Y., Shinotsuka, N., Nonomura, K., Takemoto, K., Kuida, K., Yosida, H. and Miura, M. (2011). Live imaging of apoptosis in a novel transgenic mouse highlights its role in neural tube closure. *J. Cell Biol.* **195**, 1047-1060.

Zhang, J., Wang, X., Cui, W., Wang, W., Zhang, H., Liu, L., Zhang, Z., Li, Z., Ying, G., Zhang, N. et al. (2013). Visualization of caspase-3-like activity in cells using a genetically encoded fluorescent biosensor activated by protein cleavage. *Nat. Commun.* **4**, 2157.

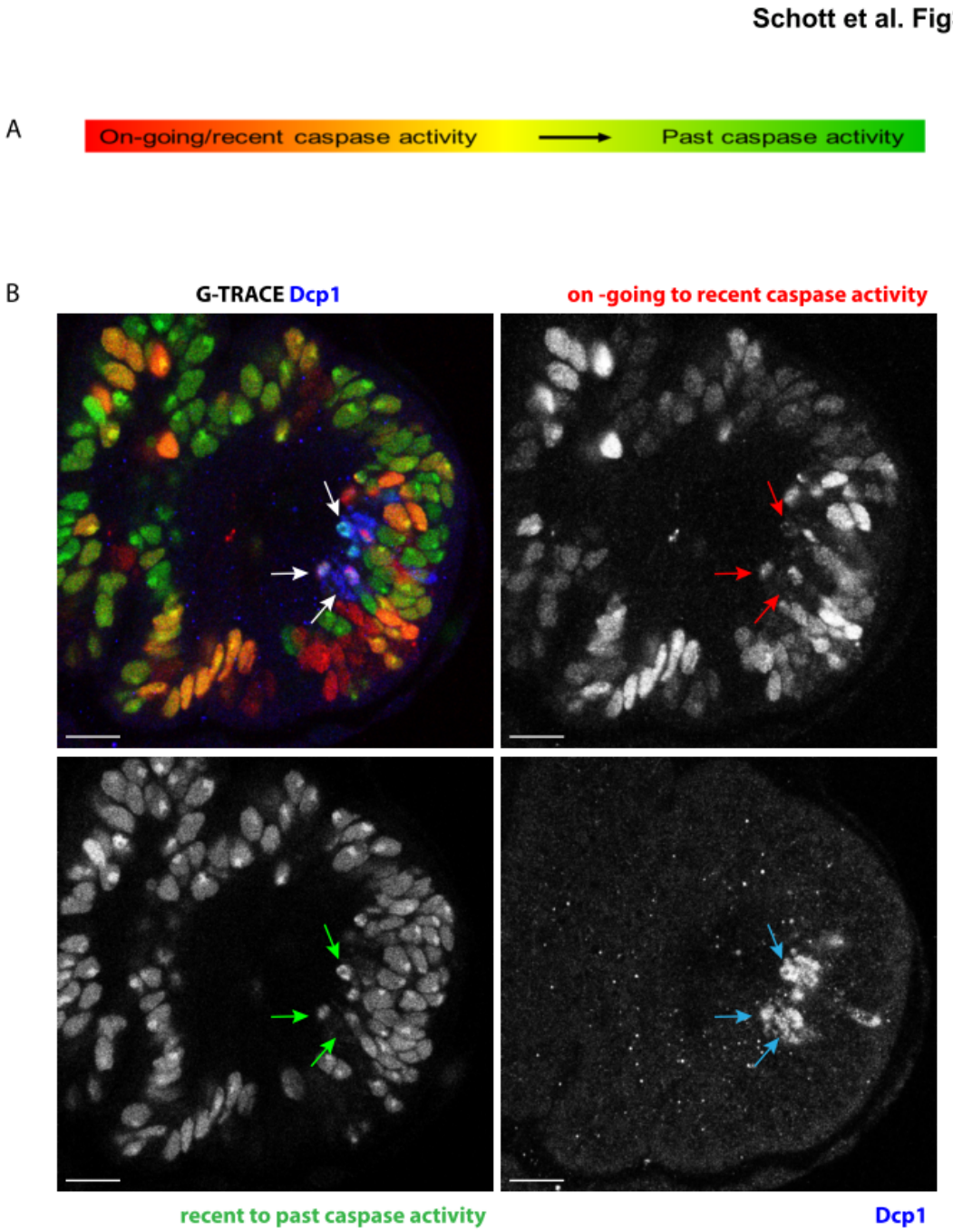

Figure S1: Activity of the caspase sensitive Gal4 sensor in the leg. A) Frieze representing the time scale labelling of caspase activity according to (Tang et al., 2015). (B) Pupal leg disc showing a wide expression of both nuclear GFP and RFP under the control of the caspase sensitive Gal4 sensor, while very few cells are positive for Dcp1 (arrows), suggesting that this caspase sensitive Gal4 can detect very low level of caspase activity, not always associated with death. Scale bar10µm, N=10.

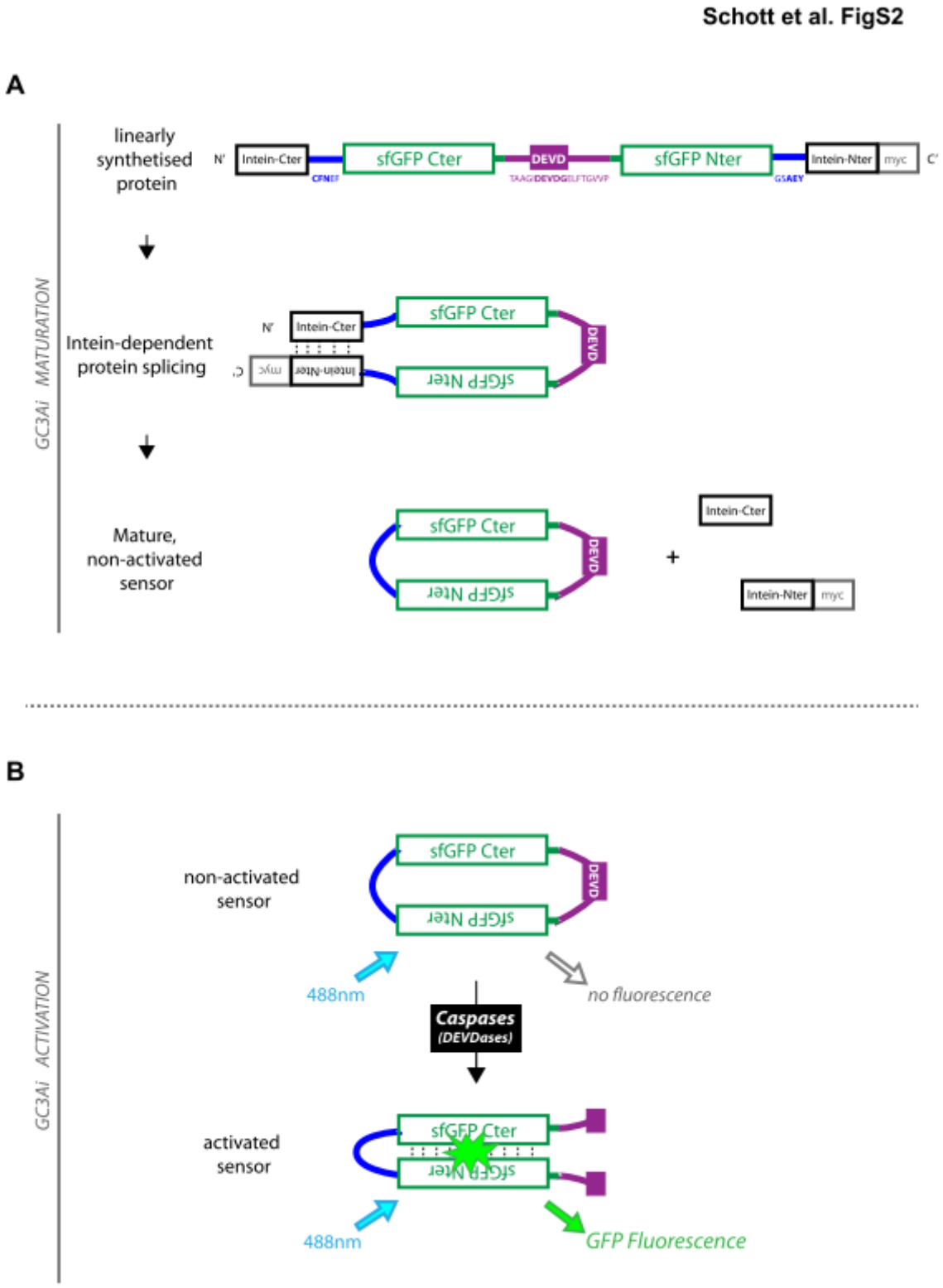

Figure S2. GC3Ai apoptosensor maturation and activation modes. Detailed scheme of the GFP sensor Caspase-3-like protease Activity Indicator (GC3Ai): the C and N termini of the GFP have been linked by a fragment containing a DEVD caspase cleavage site in such a way that DEVD needs to be cleaved in order for the GFP to fluoresce; while intein domains have been added at the new N' and C'

termini of the molecule, allowing the molecule to be circularized after intein dependent protein splicing (see (Zhang et al., 2013).

Schott et al. FigS3

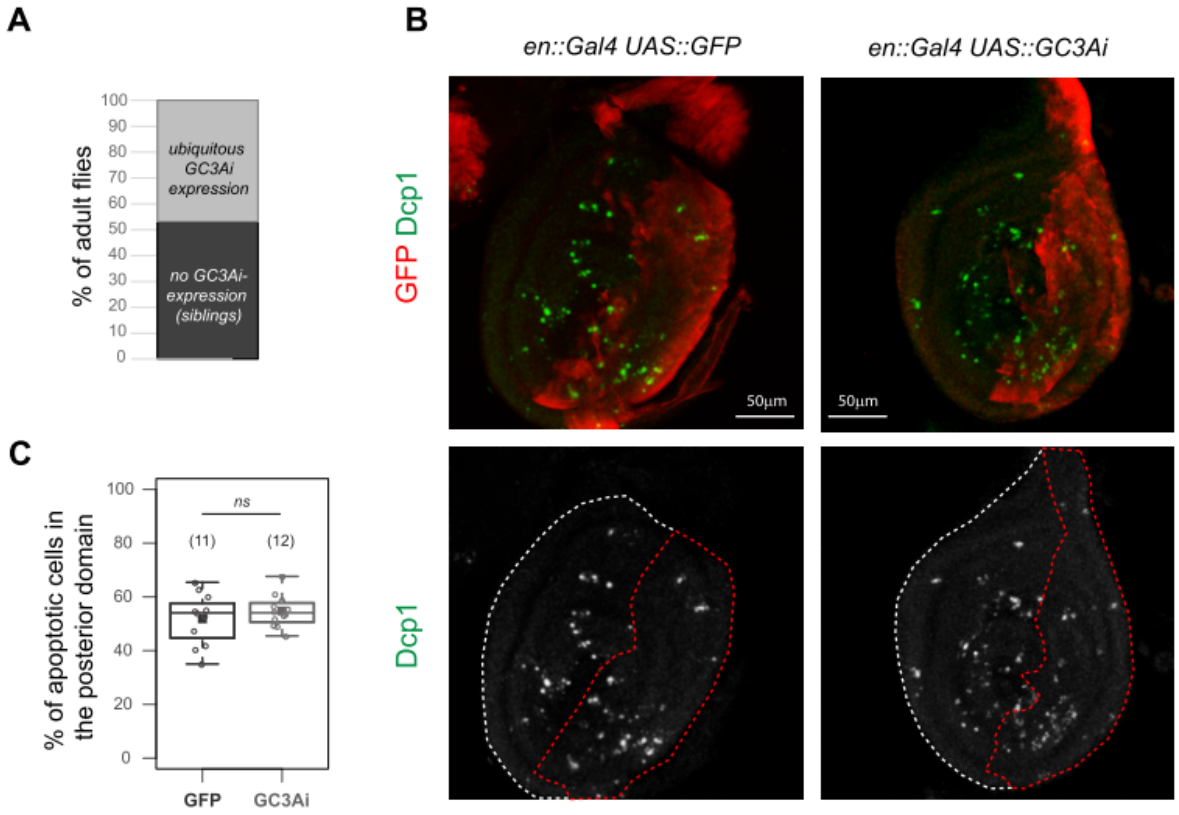

Figure S3. Effects of GC3Ai expression on viability and apoptotic pattern. (A) Comparison of the number of adult flies issued from the same cross between *act::Gal4 / CyO* and *uas::GC3Ai / uas::GC3Ai* flies (n=256 individuals in total). (B) Apoptotic pattern visualized by an anti-activated Dcp1 staining (green or white) in *en::Gal4>uas::GFP* (control) and *en::Gal4>uas::GC3Ai* leg discs. (C) Quantifications of apoptotic cells in the posterior domain (see M&M, n=11 and 12 respectively).

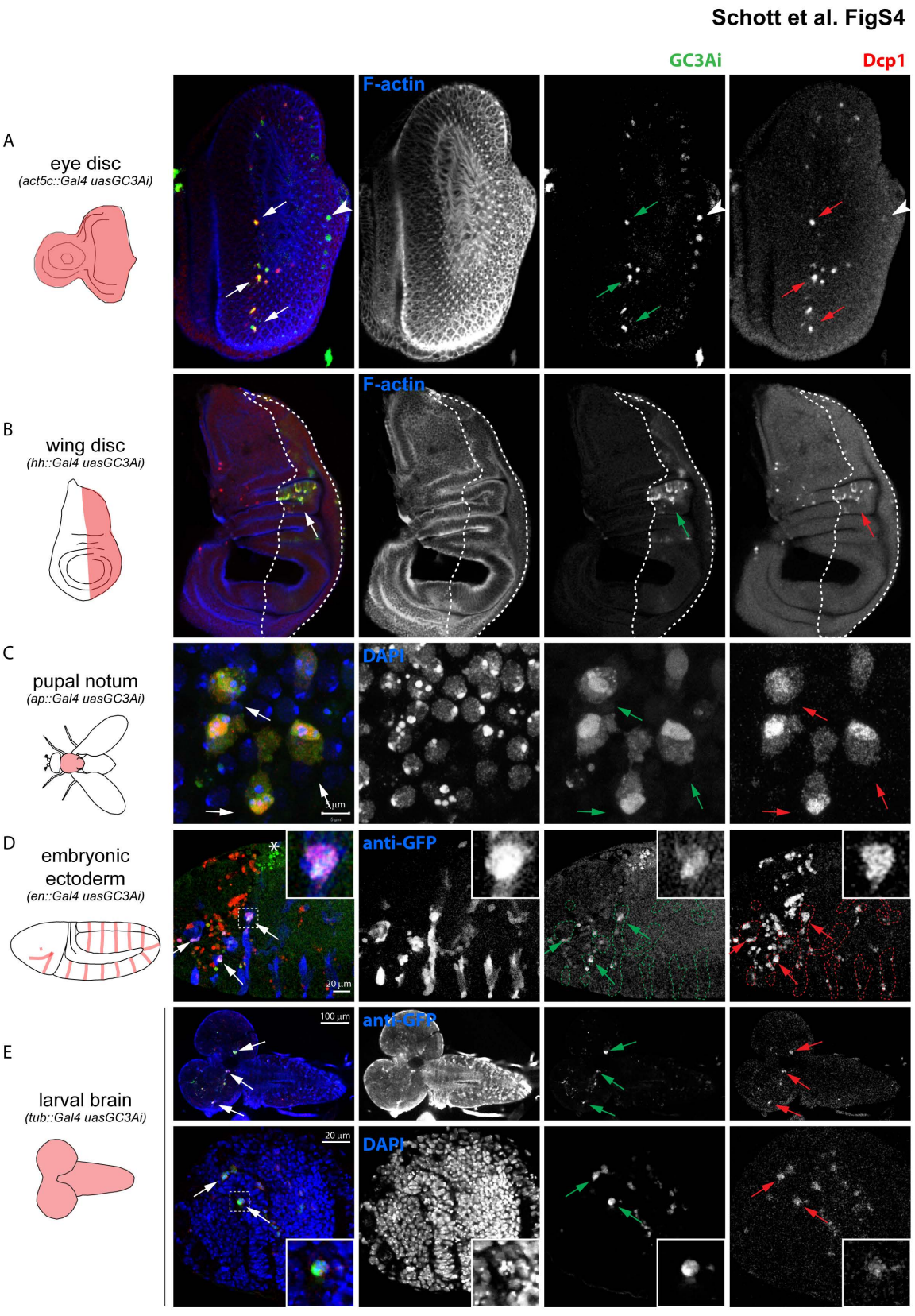

Figure S4. Pattern of GC3Ai fluorescence in various *Drosophila* tissues. (A-E) On the left are presented schemes of the different tissues showing the domain in which GC3Ai has been expressed. On the right, the GC3Ai activation pattern and activated Dcp1 antibody staining is shown. (A) Fixed eye discs (n=6) from *act::Gal4>uas::GC3Ai* L3 larvae. Note the presence of some GC3Ai positive

cells in which Dcp1 is not detectable yet, that could correspond to early apoptotic cells as shown in Fig3 (arrowhead). (B) Fixed wing imaginal discs from *hh::Gal4>uas::GC3Ai* L3 larvae (n=6). (C) Pupal notum from *ap::Gal4>uas::GC3Ai* (n=60 cells). (D) Ectoderm from *en::Gal4>uas::GC3Ai* embryos (n=8). (E) Larval central nervous system from *tub::Gal4>uas::GC3Ai* (n=7). Note the co-detection of GC3Ai and Dcp1 activation in each of these tissues (arrows).

Schott et al. FigS5

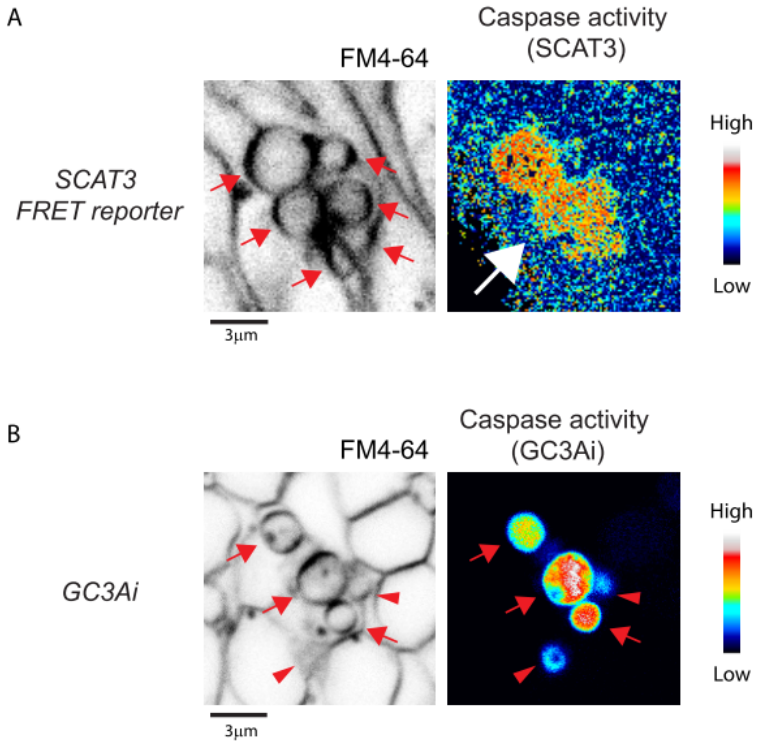

Figure S5: Caspase activity detection by SCAT3 FRET reporter and GC3Ai. A-B. Images of living tissues showing SCAT3 FRET reporter activity (A) or GC3Ai activity (B) using a color-code to report FRET ratio or fluorescence intensity. The highest intensity of caspase activity is in white while the lowest intensity is in black (see intensity scale). Labelling of the plasma membrane (black) is achieved using the lipid-binding vital dye FM4-64 which allows to detect apoptotic bodies. (A) On the left, six apoptotic bodies are detected (red arrows). On the right, the caspase activity detected by the FRET reporter highlights the dying cell (big white arrow), but individual apoptotic bodies are not clearly visible (n=15/24). (B) On the left, 3 apoptotic bodies are detected (red arrows) and on the right

GC3Ai detects all of them (red arrows) (n= 20/21). Two apoptotic bodies are slightly out of focus and indicated with arrowheads.

Schott et al. FigS6

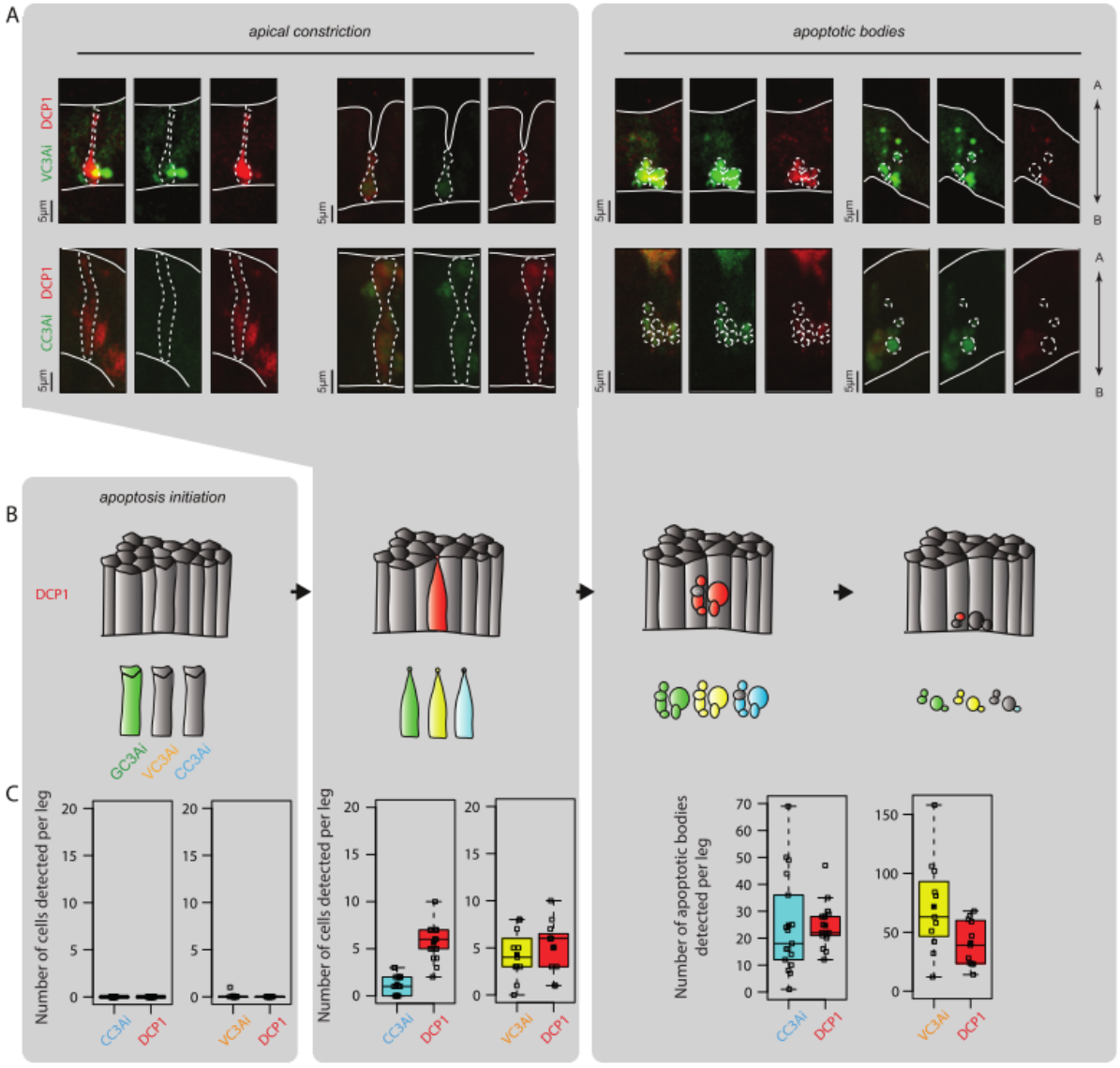

Figure S6. Pattern of fluorescence of Venus (VC3Ai) and Cerulean (CC3Ai) apoptosensors. (A-C) VC3Ai, CC3Ai and Dcp1 activation patterns are compared in pupal leg discs. Successive stages of the apoptotic process are presented from left to right. (A) Confocal images showing the comparison between VC3Ai (green), CC3Ai (green) and Dcp1 (red) activation patterns in fixed pupal leg discs at different apoptotic stages. Apoptotic cells or apoptotic bodies are surrounded by white dotted lines and the apical and basal surfaces of the epithelium are represented by a white line. (B) Schemes of the

different apoptotic stages recapitulating the activation pattern of VC3Ai (yellow) or CC3Ai (cyan) in fixed tissues, compared to Dcp1 (red). The pattern of GC3Ai fluorescence, as determined on fixed tissues in figure 3, is shown in green for comparison. (C) Quantification of the number of VC3Ai (yellow), CC3Ai (cyan) and Dcp1 (red) positive apoptotic cells or apoptotic bodies counted per fixed leg disc according to the different apoptotic stages (n=11 legs for VC3Ai, n=17 legs for CC3Ai). Data are presented as box plots showing every leg disc (open squares) as well as the mean (filled square).

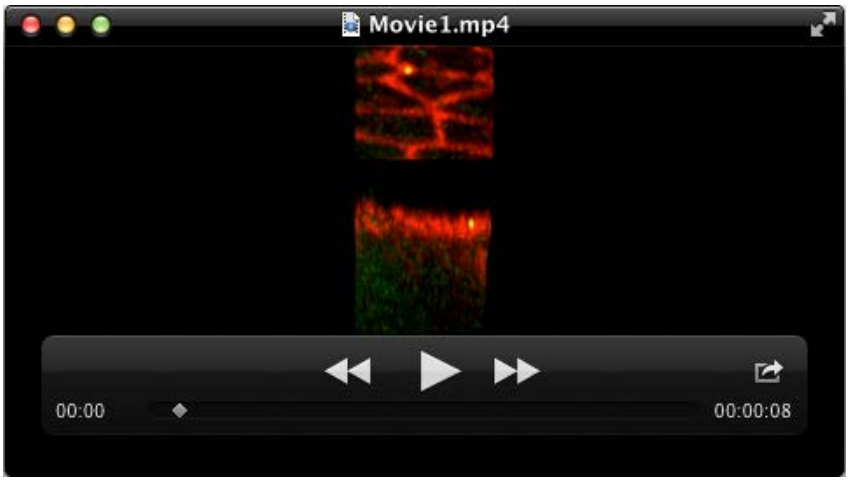

Movie 1. Time lapse of a subset of a pupal leg disc expressing alphaCat-TagRFP in the ap domain (which encompasses the t4-t5 fold) and the GC3Ai construct to reveal caspase activity and thus visualise apoptotic cell. The apoptotic cell shape can be followed on the apical (top) and sagittal (bottom) sections. Note the reduction of the apical surface of the apoptotic cell on the apical views, the transient deformation of the apical surface on the sagittal views and the formation of apoptotic bodies.